

# SIMULATION MODEL FOR TRANSVERSAL LOOP OSCILLATIONS: THE EFFECTS INDUCED BY SHOCK WAVES AND OPPOSITION OF THE EXTERNAL MEDIUM

GABRIELA R. MOCANU, ALEXANDRU MARCU

*Babeş-Bolyai University, Faculty of Physics,  
Department of Theoretical and Computational Physics,  
Cluj-Napoca, România.*

*Email: gabriela.mocanu@ubbcluj.ro, alexandru.marcu@phys.ubbcluj.ro*

*Abstract.* The EUV imaging telescope onboard the Transition Region And Coronal Explorer (TRACE) spacecraft provided observations with high spatial resolution and unprecedented time cadence of spatial oscillations of solar coronal loops. Current theoretical models attempt to explain the excitation mechanism, rapid damping and selectivity of these oscillations. The theoretical model presented here simulates the interaction between a magnetic slab and a finite width shock wave generated by a nearby explosive flare event. The slab has an exponential density stratification, with variable hydrostatic scale height. As a key feature, the subsequent observed damping is considered to occur due to the opposition of the external magnetized medium to the perpendicular propagation of a medium/low velocity disturbance. Comparison of the theoretical damping results of the model with observational data gives an excellent agreement.

*Key words:* Corona, Structures; Coronal Seismology; Magnetic fields, Corona..

## 1. INTRODUCTION

High resolution observations supplied by TRACE/EUV in the  $171\text{\AA}$  and  $195\text{\AA}$  filters show spatial displacement of solar coronal loops [1, 2, 11, 20]. They are dubbed "transversal modes", as it is observed that the plasma inside the loop moves as a whole perpendicular to the equilibrium magnetic field which is aligned with the symmetry axis of magnetic structures. These oscillations are considered to be triggered by massive nearby releases of energy, such as flares, CMEs or filament destabilization. Based even on visual inspection only \*, it is clear that the loops' foot points are not displaced considerably and that the oscillations damp on time scales comparable to the loops' oscillations period. Another puzzling observational fact is that only a small percent of the flares show oscillating loops [2].

The theoretical models developed in the last few years attempted to give valid explanations for the value of periods and damping times and also to explain the excitation mechanism and the selectivity of loops excitation. Several theoretical mod-

\*Full movies of the events are available, by courtesy of [20], at <http://vestige.lmsal.com/TRACE/POD/TRACEoscillations.html>.

els were proposed to explain the excitation and damping of oscillations, including viscous damping with anomalous low Reynolds number [11], damping due to phase mixing [16], destabilization of magnetic sources in the photosphere and damping due to subsequent relaxation of magnetic field lines [19], damping due to foot point leakage of Alfvén waves [8], damping due to resonant absorption [17], viscous damping due sub resolution scales [15], excitation and damping due to dispersive nature of the magnetized medium inside and outside the loop [21], excitation due to vortex shedding [13]. The common aspects of these models are the association of a flare event with the excitation and the identification of the oscillation mode as the fast kink mode of a magnetic flux tube [11]. Once the oscillations of loops became observable and this motion was quantified a new branch of solar physics called *coronal magneto-seismology* became possible [4, 5, 9, 7, 11, 3, 12, 10]. This remote diagnostic tool deepened our understanding of the dynamics of the solar corona, its stability and thermal state. New observations made recently by Hinode and SDO will revolutionize almost the entire solar physics.

One of the fundamental ideas employed by our study resides in the consideration of the excitation mechanism to be due to a shock wave travelling towards the loop. The shock itself can be generated by a nearby flare. The observed geometry of the incident wave-loop system (i.e. the external disturbance travels perpendicular to the external magnetic field) drives us to believe that the shock wave is a fast magneto acoustic shock. Following the impact, the loop begins to oscillate and the reported maximum velocity amplitude is of the order of 10 km/s [2, 20]. The damping of the induced oscillations occurs as a result of the opposition of the external magnetized medium to a transversal slowly propagating oscillation. The analytical treatment is carried out without using the mathematical constraint that the mode might be a kink mode. This approach is also supported by latest modelling of observational data [24]. For our study the only condition applied is that the solution satisfies the observed boundary condition of fixed foot points. In Section 2 we develop the mathematical treatment necessary for our study, while in Section 3 the results are presented and discussed. Conclusions follow in Section 4.

## 2. MATHEMATICAL APPROACH

The configuration under analysis consists of a magnetic slab approximating the line tied coronal loop. In a coordinate system fixed to the loop, the structure is aligned with its constant equilibrium magnetic field  $\mathbf{B}_0$  and the  $-\hat{\mathbf{z}}$  axis (Fig. 1). The internal and external magnetic fields are of the same order of magnitude and if they not parallel, they are at least coplanar in the  $yOz$  plane. The shock wave, moving parallel to the  $x$  axis, hits the loop and exerts a force  $\mathbf{F}_{sh}$ . The response of

the external medium to the oscillations of the loop is given through a force of the form  $\mathbf{F}_{ext} = -\alpha\mathbf{v}$  where  $\alpha$  is a constant and  $\mathbf{v}$  is the velocity of the oscillating loop.

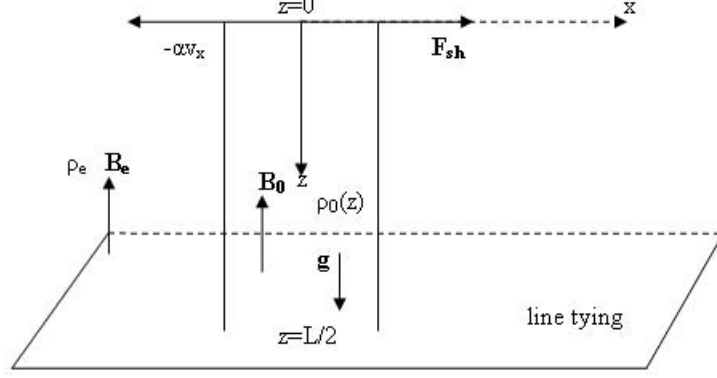


Fig. 1 – Geometrical configuration of the model.

In order to simplify our analysis we will use the  $\beta \rightarrow 0$  approximation which still preserves the important physics involved in the problem.

Observations of transversal displacements place the value of the maximum velocity amplitude two orders of magnitude smaller than the local Alfvén speed. In the following mathematical treatment this observational fact is translated into the use of linear magnetohydrodynamics (MHD) theory.

The set of linear and ideal MHD equations, in the  $\beta \rightarrow 0$  approximation is given by

$$\begin{aligned} \frac{\partial \rho}{\partial t} + \nabla \cdot (\rho_0(z)\mathbf{v}) &= 0, \\ \rho_0(z) \frac{\partial \mathbf{v}}{\partial t} &= \frac{1}{\mu_0} (\nabla \times \mathbf{B}) \times \mathbf{B}_0 + \rho \mathbf{g} + \mathbf{F}_{sh} - \alpha \mathbf{v}, \\ \frac{\partial \mathbf{B}}{\partial t} &= \nabla \times (\mathbf{v} \times \mathbf{B}_0), \\ \nabla \cdot \mathbf{B} &= 0, \end{aligned} \quad (1)$$

where  $\rho_0(z) = \rho_{00}f(z)$  is the equilibrium density of the internal medium,  $\rho_{00}$  is the density in the apex of the loop,  $\mathbf{g} = g\hat{\mathbf{z}}$  is the gravitational acceleration, and  $\rho, \mathbf{v}, \mathbf{B}$  denote the perturbations of the pressure, density, velocity and magnetic field.

We assume a two-dimensional dynamics, neglecting changes in the  $y$  direction. We can solve the system of equations for the perturbed velocities,  $v_x = \mathbf{v} \cdot \hat{\mathbf{x}}$  and  $v_z = \mathbf{v} \cdot \hat{\mathbf{z}}$ , and it follows that the equations describing the dynamics of the loop are

$$f(z) \frac{\partial^2 v_x}{\partial t^2} = v_{A0}^2 \frac{\partial^2 v_x}{\partial z^2} + \frac{1}{\rho_{00}} \frac{\partial F_{sh}}{\partial t} - \frac{\alpha}{\rho_{00}} \frac{\partial v_x}{\partial t}, \quad (2)$$

$$f(z) \frac{\partial^2 v_z}{\partial t^2} = \frac{\alpha}{\rho_{00}} \frac{\partial v_z}{\partial t} - g f(z) \frac{\partial v_z}{\partial z} - g v_z \frac{df(z)}{dz}, \quad (3)$$

where  $v_{A0}^2 = B_0^2/(\mu_0 \rho_{00})$  is the Alfvén speed measured in the apex of the coronal loop.

We tackle the problem as it would consist of two superimposed **independent** processes, discussed below.

1. Longitudinal wave propagation: this part of the process is considered to be known and is modelled as a decaying propagating plane wave of the form

$$v_z = \widehat{v}_z e^{i(\omega_z t + k_z z)}, \quad (4)$$

where  $\omega_z \in \mathbf{R}$ ,  $k_z \in \mathbf{C}$ . Our choice is based on the observational fact that longitudinal oscillations are seen to damp on a very short spatial scale [6]. This scale is much shorter than the typical spatial scale arising from density stratification, thus making it possible for us to use Fourier analysis to describe the longitudinal oscillation process.

2. Transversal wave propagation: we wish to discuss and consider this phenomenon as unknown and from now we will model it as a time decaying oscillation

$$v_x = \widehat{v}_x(z) e^{i\omega t}, \quad (5)$$

where

$$\omega = \omega_R + i\omega_I. \quad (6)$$

The values for  $\omega_R$  are given by the observed oscillation periods. In the numerical calculations, when the time evolution of each loop is considered,  $\omega_R$  will be replaced by  $2\pi/P$ , where  $P$  is the reported oscillations period of the loop. A non-zero complex frequency,  $\omega_I$ , allows for a numerical treatment of the observed temporal decay of oscillations.

If Eqs (2) and (3) are analyzed, it might be argued that the two velocities are not independent as they both depend on  $\alpha$ . However, if starting from Eq. (3) and imposing that  $v_z$  has accepted observational values for longitudinal propagation, the  $\alpha$  coefficient is almost constant (Fig. 2) and is not responsible for an effective coupling between the longitudinal and transversal oscillations.

Using Eqs (4) and (5), we can solve Eq. (3) for  $\alpha$ . Introducing this result back into Eq. (2) we obtain the evolutionary equation for  $\widehat{v}_x$  as

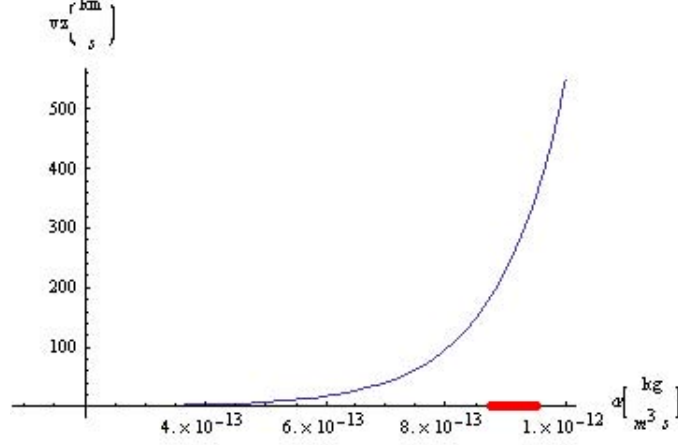


Fig. 2 – Variation of the longitudinal velocity as a function of the  $\alpha$  coefficient. The interval in red maps the values of  $\alpha$  that lead to longitudinal velocities consistent with observations.

$$f(z)\omega^2\hat{v}_x + v_{A0}^2 \frac{d^2\hat{v}_x}{dz^2} = -\frac{1}{\rho_{00}} \frac{\partial F_{sh}}{\partial t} e^{-i\omega t} + \frac{\omega}{\omega_z} \hat{v}_x \left[ -\omega_z^2 f(z) + ik_z g f(z) + g \frac{df(z)}{dz} \right], \quad (7)$$

This equation can be separated into its real and imaginary part, where the real part can be given as

$$\begin{aligned} v_{A0}^2 \frac{d^2\hat{v}_x}{dz^2} + \hat{v}_x \left[ f(z) \left( \omega_R^2 - \omega_I^2 + \omega_R \omega_z + g \frac{\omega_R}{\omega_z} k_z \right) - \frac{\omega_R}{\omega_z} g \frac{df(z)}{dz} \right] \\ = -\frac{1}{\rho_{00}} \frac{\partial F_{sh}}{\partial t} e^{\omega_I t} \cos(\omega_R t). \end{aligned} \quad (8)$$

The analytical form of  $F_{sh}$  must account for the short temporal interaction and the localized spatial impact. We assume that the shock wave hits both feet of the loop at the same time (i.e. there is no phase delay). These suppositions can be modelled by using a Heaviside step function for the time dependence and a Gaussian centered on the point of impact for the space dependence of the incoming driver, therefore  $\mathbf{F}_{sh}(z, t)$  will be considered to be of the form

$$\begin{aligned} \mathbf{F}_{sh}(z, t) &= F(z, t) \hat{\mathbf{x}}, \\ F(z, t) &= F_0 H(\tau - t) \frac{1}{a\sqrt{\pi}} \left[ e^{-(z-z_0)^2/a^2} + e^{-(z+z_0)^2/a^2} \right], \end{aligned} \quad (9)$$

where  $F_0$  is the energy per appropriate length scale of the fast MHD shock wave, given as  $F_0 = 1/2\rho_e c(v_{Ae}^2 + c_{Se}^2)/a$ ,  $c$  is a constant used to determine the amount

of energy needed to obtain the observed displacements,  $\tau$  is the temporal duration of the interaction,  $a$  is the width of the spatial shock and  $z_0$  and  $-z_0$  are the impact points along the two sides of the loop. Other variables are taken as  $\rho_e = d \cdot \rho_{00}$ ,  $c_{Se} = 10^5 m/s$ ,  $v_{Ae} = v_{A0} \sqrt{(1/d)}$ , with  $d$  being the density filling factor of the loop.

### 3. RESULTS AND DISCUSSION

The analysis is restricted to only one half of the loop, namely for  $z \in [0, L/2]$ , and symmetry is assumed for the other half. The symmetry assumption of our model is valid since the  $\alpha$  coefficient is constant and there is no temporal delay between the interaction of the shock wave with the two feet of the loop.

Having in mind this simplification, Eq. (9) is modified as

$$F(z, t) = F_0 H(\tau - t) \frac{1}{2a\sqrt{\pi}} e^{-(z-z_0)^2/a^2}. \quad (10)$$

The density profile described by the function  $f(z)$  is taken to be an exponential function of  $z$ , decaying towards the apex. This choice of the density dependence with height was earlier employed by many authors [22, 18] and is based on the study of 30 loops observed by SoHO/EIT [1]. [18] include a sinusoidal function in the argument of the exponent, to ensure symmetry in a cylindrical configuration. This sinusoidal inclusion is, however, not applicable for the slab configuration used in this model. In particular, the variation of the equilibrium density with height becomes

$$f_n(z) = e^{nz/L}. \quad (11)$$

where the dimensionless number  $n$  is a parameter standing for variable scale height along the loop.

Solving Eq. (8), the spatial dependence of the transversal velocity is obtained to be of the form

$$\hat{v}_x = T_0(t) \sum_{i=1}^{i=12} T_i(z), \quad (12)$$

where  $T_i(z)$  are complicated function containing combinations of Bessel functions (see Appendix A).

The next step of our analysis is to determine the temporal evolution of the displacement of the apex of the loop, for different impact points along the loop and considering different values for  $n$ . For example, for loop $_i$ , ( $i = 1 \dots 12$ ), we set values for  $z_0$  and  $n$  (for example  $z_0 = L/8$  and  $n = 2$ ). Next, we fit the values for  $c$  and  $\omega_I$  in such a way that

1. the resulting apex displacement is equal to the observed value, i.e. to 0.8 Mm for loop 1 (see observational data collected in Table 1).
2. the displacement after  $t_d$ , i.e. after 1200 seconds, corresponds to an e-folding decay of the maximum amplitude.

From the large number of oscillations discussed in the literature, we selected a few events (presented in Table 1) satisfying a few imposed criteria, e.g. the flare had to be near the loop, but not localized at one of its foot points or underneath it. We also neglected those reported oscillations where uncertainties in observational data were large.

Calculations are performed for  $d = 0.1$ . Using numerical simulations first we obtained that a variation of  $d$  in the interval  $(0, 1]$  does not have any significant effect on the obtained results and so, there is no relation between the observed displacement and density ratio that can be used in the seismological investigation of the present study.

This simple algorithm was applied to loops 1 – 7 and 12, for which all the needed data can be extracted from observations. For each loop,  $c$  and  $\omega_I$  were fitted for combinations of the parameters  $n$  and  $z_0$ , as seen in Tables 2-9. At this point we would wish to discuss one of the details of the calculations. Initially, the sign of  $\omega_I$  was not fixed (i.e. to positive or negative) and it was found that, within the framework of this model and in order to obtain the observational damping time,  $\omega_I$  had to be negative. Combining this fact with equation 5 one would formally obtain an exponential growth and not a decay. But in the particular case of this model, the superposition of all the effects, the  $-\alpha v$  term and the shock term do not allow for a growth instability to occur. We redid all the calculations with  $\omega_I$  positive and only at this point we obtained a behavior that leads to instability. We propose that this may be explained if one looks carefully at the right hand side of Eq. 8. The driving term is multiplied by the time exponential  $e^{\omega_I t}$ . If the values of  $\omega_I$  were positive, this term would grow exponentially leading to an instability.

For every loop, we plotted the displacement of the loop apex as a function of time. The agreement with observational data [2, 20] is very good (see Figures 4 and 6 for theoretical predictions of time evolutions of loops 14 and 6 respectively and Figures 3 [2] and 5 [2] for their observed evolution).

The time evolution of loop 12 is presented in Fig. 8 and it is compared to the observational fit [23], Fig. 7.

The following type of analysis is done with calibration purposes. We will set the values for  $z_0$  and  $n$  at  $L/8$  and 2 respectively. For these fixed parameters we retrieve the corresponding optimum values for  $c$  and  $\omega_I$  from one of the Tables 2-9. At this point we allow  $z_0$  and  $n$  to vary again to see in what way this variation affects the optimum prescribed theoretical behavior.

Table 1

The observational and computed data for 12 loops  
 Only data for loops 1-7 and 12 were complete, so for these loops our analysis is accurate  
 A denotes the maximum observed amplitude of oscillations

	L[Mm]	P[s]	$t_d$ [s]	A[Mm]	$v_A$ [km/s]
1 <sup>a</sup>	168	261	1200	0.8	2600
2 <sup>b</sup>	72	265	300	2	2600
3 <sup>c</sup>	174	316	500	6	2600
4 <sup>d</sup>	204	277	400	4	2500
5 <sup>e</sup>	162	272	849	5	3000
6 <sup>f</sup>	258	435	600	0.7	2500
7 <sup>g</sup>	146	396	400	1.8	3500
8 <sup>h</sup>	258	435	600	-	839
9 <sup>i</sup>	166	143	200	-	1640
10 <sup>j</sup>	406	423	800	-	1360
11 <sup>k</sup>	192	185	200	-	1470
12 <sup>l</sup>	340	630	1000	4	2000

1<sup>a</sup> previously described in [2, 20],  
 triggered by a M4.6 flare, event on 14 July 1998,  
 12:45 UT, their loop 1a.

2<sup>b</sup> (idem 1<sup>a</sup>), their loop 1b.

3<sup>c</sup> (idem 1<sup>a</sup>), their loop 1d.

4<sup>d</sup> (idem 1<sup>a</sup>), their loop 1f.

5<sup>e</sup> (idem 1<sup>a</sup>), their loop 1g.

6<sup>f</sup> previously described by [2, 20],  
 event on 4 Jul 1999, 08.33 UT, triggered by a C4.6  
 flare, their loop 4a.

7<sup>g</sup> previously described by [2, 20],  
 event on 15 Jun 2001, 06:35 UT, triggered by a

C3.8 flare, their loop 17a.

8<sup>h</sup> previously described by [14],  
 event on 4 Jul 1999, their loop 7.

9<sup>i</sup> previously described by [14],  
 event on 25 Oct 1999, their loop 8.

10<sup>j</sup> previously described by [14],  
 event on 21 Mar 2001, their loop 9.

11<sup>k</sup> previously described by [14],  
 event on 15 May 2001, their loop 10.

12<sup>l</sup> previously described by [23],  
 event on 27 Jun 2007, triggered by a C1.3 flare.

Table 2

Numerical data for loop 1, with  $\omega_I$  in units of  $s^{-1}$

	$z_0 = 0$	$z_0 = L/8$	$z_0 = L/4$
$n = 0$	$c = 0.498$ $\omega_I = -6.65 \cdot 10^{-4}$	$c = 0.294$ $\omega_I = -6.66 \cdot 10^{-4}$	$c = 0.408$ $\omega_I = -6.66 \cdot 10^{-4}$
$n = 1$	$c = 0.385$ $\omega_I = -6.65 \cdot 10^{-4}$	$c = 0.222$ $\omega_I = -6.65 \cdot 10^{-4}$	$c = 0.298$ $\omega_I = -6.65 \cdot 10^{-4}$
$n = 2$	$c = 0.2275$ $\omega_I = -6.65 \cdot 10^{-4}$	$c = 0.127$ $\omega_I = -6.65 \cdot 10^{-4}$	$c = 0.164$ $\omega_I = -6.65 \cdot 10^{-4}$

Table 3

Numerical data for loop 2, with  $\omega_I$  in units of  $s^{-1}$ 

	$z_0 = 0$	$z_0 = L/8$	$z_0 = L/4$
$n = 0$	$c = 5.85$ $\omega_I = -20.25 \cdot 10^{-4}$	$c = 3.76$ $\omega_I = -20.25 \cdot 10^{-4}$	$c = 5.58$ $\omega_I = -20.28 \cdot 10^{-4}$
$n = 1$	$c = 5.78$ $\omega_I = -20.28 \cdot 10^{-4}$	$c = 3.7$ $\omega_I = -20.28 \cdot 10^{-4}$	$c = 5.45$ $\omega_I = -20.28 \cdot 10^{-4}$
$n = 2$	$c = 5.65$ $\omega_I = -20.23 \cdot 10^{-4}$	$c = 3.62$ $\omega_I = -20.23 \cdot 10^{-4}$	$c = 5.3$ $\omega_I = -20.23 \cdot 10^{-4}$

Table 4

Numerical data for loop 3, with  $\omega_I$  in units of  $s^{-1}$ 

	$z_0 = 0$	$z_0 = L/8$	$z_0 = L/4$
$n = 0$	$c = 3.155$ $\omega_I = -17.2 \cdot 10^{-4}$	$c = 1.91$ $\omega_I = -17.2 \cdot 10^{-4}$	$c = 2.685$ $\omega_I = -17.2 \cdot 10^{-4}$
$n = 1$	$c = 2.75$ $\omega_I = -17.2 \cdot 10^{-4}$	$c = 1.632$ $\omega_I = -17.2 \cdot 10^{-4}$	$c = 2.25$ $\omega_I = -17.2 \cdot 10^{-4}$
$n = 2$	$c = 2.195$ $\omega_I = -17.2 \cdot 10^{-4}$	$c = 1.27$ $\omega_I = -17.2 \cdot 10^{-4}$	$c = 1.702$ $\omega_I = -17.2 \cdot 10^{-4}$

Table 5

Numerical data for loop 4, with  $\omega_I$  in units of  $s^{-1}$ 

	$z_0 = 0$	$z_0 = L/8$	$z_0 = L/4$
$n = 0$	$c = 0.61$ $\omega_I = -23.45 \cdot 10^{-4}$	$c = 0.34$ $\omega_I = -23.45 \cdot 10^{-4}$	$c = 0.453$ $\omega_I = -23.45 \cdot 10^{-4}$
$n = 1$	$c = 0.113$ $\omega_I = -23.45 \cdot 10^{-4}$	$c = 0.0602$ $\omega_I = -23.42 \cdot 10^{-4}$	$c = 0.077$ $\omega_I = -23.42 \cdot 10^{-4}$
$n = 2$	$c = 1.215$ $\omega_I = -23.42 \cdot 10^{-4}$	$c = 0.608$ $\omega_I = -23.42 \cdot 10^{-4}$	$c = 0.733$ $\omega_I = -23.42 \cdot 10^{-4}$

Table 6

Numerical data for loop 5, with  $\omega_I$  in units of  $s^{-1}$ 

	$z_0 = 0$	$z_0 = L/8$	$z_0 = L/4$
$n = 0$	$c = 4.37$ $\omega_I = -7.96 \cdot 10^{-4}$	$c = 3.225$ $\omega_I = -7.96 \cdot 10^{-4}$	$c = 3.83$ $\omega_I = -7.96 \cdot 10^{-4}$
$n = 1$	$c = 3.985$ $\omega_I = -7.96 \cdot 10^{-4}$	$c = 2.415$ $\omega_I = -7.96 \cdot 10^{-4}$	$c = 3.375$ $\omega_I = -7.96 \cdot 10^{-4}$
$n = 2$	$c = 3.48$ $\omega_I = -7.97 \cdot 10^{-4}$	$c = 2.065$ $\omega_I = -7.97 \cdot 10^{-4}$	$c = 2.825$ $\omega_I = -7.96 \cdot 10^{-4}$

Table 7

Numerical data for loop 6, with  $\omega_I$  in units of  $s^{-1}$ 

	$z_0 = 0$	$z_0 = L/8$	$z_0 = L/4$
$n = 0$	$c = 0.0682$ $\omega_I = -11.33 \cdot 10^{-4}$	$c = 0.03908$ $\omega_I = -11.33 \cdot 10^{-4}$	$c = 0.053$ $\omega_I = -11.33 \cdot 10^{-4}$
$n = 1$	$c = 0.037$ $\omega_I = -11.33 \cdot 10^{-4}$	$c = 0.205$ $\omega_I = -11.33 \cdot 10^{-4}$	$c = 0.0269$ $\omega_I = -11.33 \cdot 10^{-4}$
$n = 2$	$c = 0.00844$ $\omega_I = -11.33 \cdot 10^{-4}$	$c = 0.00445$ $\omega_I = -11.33 \cdot 10^{-4}$	$c = 0.00557$ $\omega_I = -11.33 \cdot 10^{-4}$

Table 8

Numerical data for loop 7, with  $\omega_I$  in units of  $s^{-1}$ 

	$z_0 = 0$	$z_0 = L/8$	$z_0 = L/4$
$n = 0$	$c = 4.048$ $\omega_I = -24.95 \cdot 10^{-4}$	$c = 2.626$ $\omega_I = -24.95 \cdot 10^{-4}$	$c = 3.932$ $\omega_I = -24.95 \cdot 10^{-4}$
$n = 1$	$c = 4.04$ $\omega_I = -24.95 \cdot 10^{-4}$	$c = 2.6215$ $\omega_I = -24.95 \cdot 10^{-4}$	$c = 3.922$ $\omega_I = -24.95 \cdot 10^{-4}$
$n = 2$	$c = 4.033$ $\omega_I = -24.95 \cdot 10^{-4}$	$c = 2.615$ $\omega_I = -24.95 \cdot 10^{-4}$	$c = 3.912$ $\omega_I = -24.95 \cdot 10^{-4}$

Table 9

Numerical data for loop 12, with  $\omega_I$  in units of  $s^{-1}$ 

	$z_0 = 0$	$z_0 = L/8$	$z_0 = L/4$
$n = 0$	$c = 0.248$ $\omega_I = -8.41 \cdot 10^{-4}$	$c = 0.1216$ $\omega_I = -8.41 \cdot 10^{-4}$	$c = 0.15$ $\omega_I = -8.41 \cdot 10^{-4}$
$n = 1$	$c = 0.453$ $\omega_I = -8.41 \cdot 10^{-4}$	$c = 0.203$ $\omega_I = -8.42 \cdot 10^{-4}$	$c = 0.232$ $\omega_I = -8.41 \cdot 10^{-4}$
$n = 2$	$c = 0.851$ $\omega_I = -8.42 \cdot 10^{-4}$	$c = 0.3245$ $\omega_I = -8.41 \cdot 10^{-4}$	$c = 0.3335$ $\omega_I = -8.41 \cdot 10^{-4}$

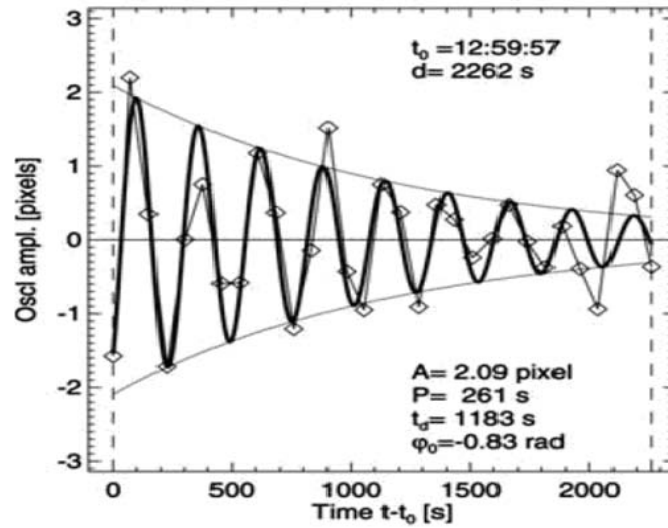


Fig. 3 – Amplitude of the apex displacement for loop 1 deduced by fitting observational points with a damped oscillation.

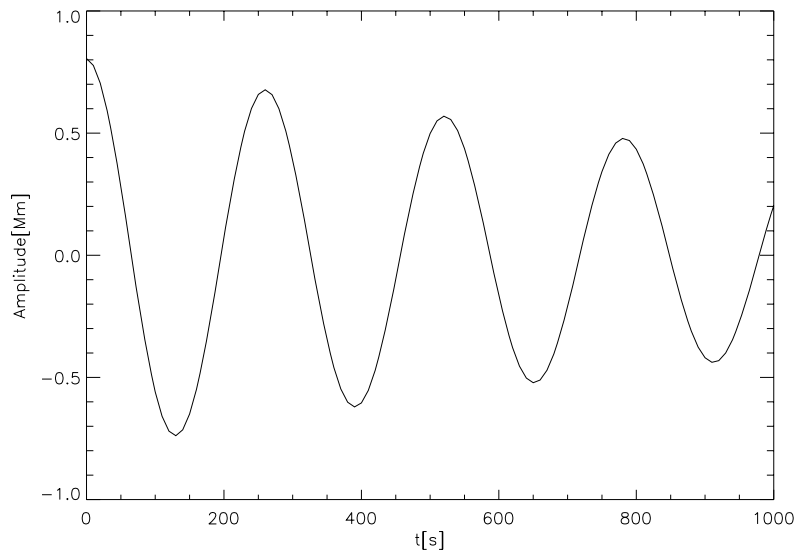


Fig. 4 – Amplitude of the apex displacement of loop 1 according to our model, with  $n = 2$  and  $z_0 = L/8$ .

If all parameters are held fixed and the values for  $c$  and  $\omega_I$  are those fitted for  $n = 2$  and  $z_0 = L/8$ , then the variation of the apex displacement as a function of  $n$  has the profile presented in Figure 9, in the case of loop 6. The sharp peak at  $n = 2$

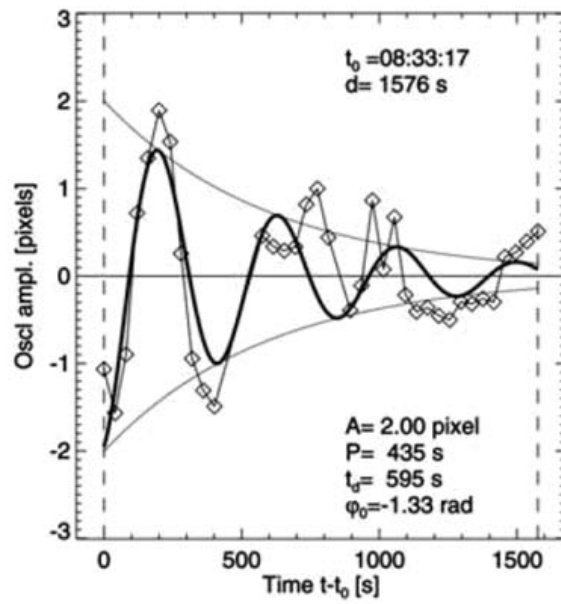


Fig. 5 – Amplitude of the apex displacement for loop 6 deduced by fitting observational points with a damped oscillation.

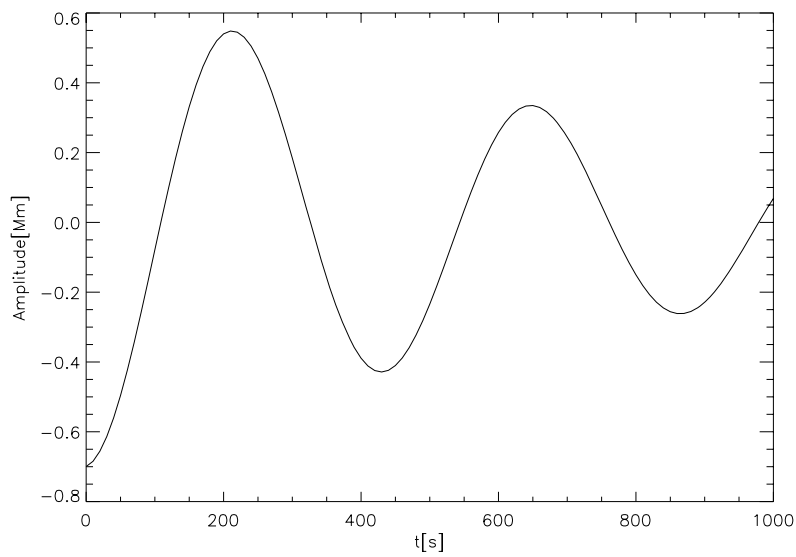


Fig. 6 – Amplitude of the apex displacement for loop 6 according to our model, with  $n = 2$  and  $z_0 = L/8$ .

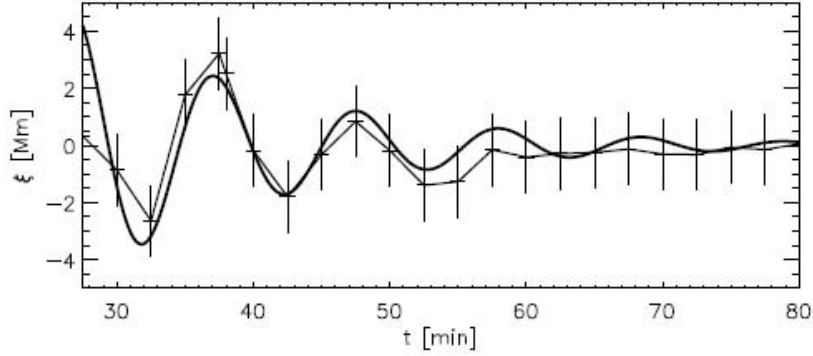


Fig. 7 – Amplitude of the apex displacement for loop 12 deduced by fitting observational points with a damped oscillation.

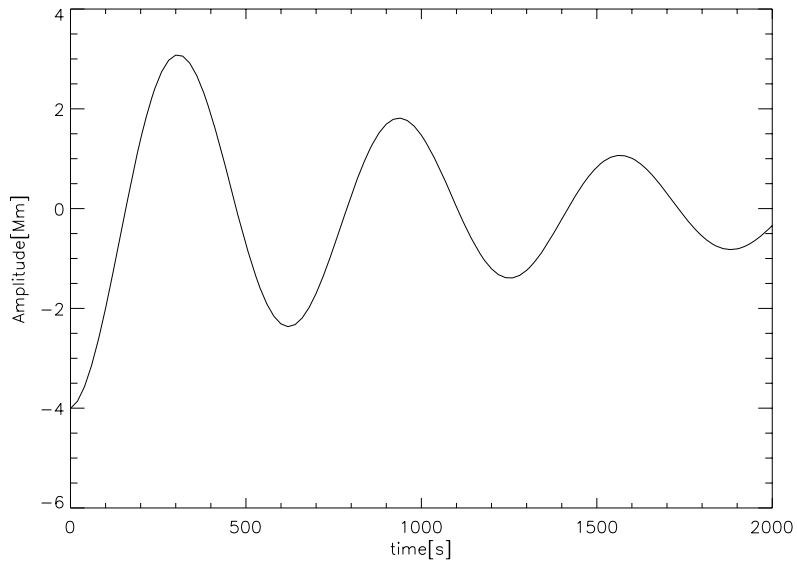


Fig. 8 – Amplitude of the apex displacement of loop 12 according to our model, with  $n = 2$  and  $z_0 = L/8$ .

is explained because the free parameters were fitted such that  $n = 2$  is the optimum case. It can also be seen that for a specific value of  $n$  the amplitude can change sign, i.e. there is a certain combination of parameters such that the variation of  $n$  leads to a change in the polarization of the oscillation.

In the case of loop 1 we keep all parameters fixed and the values for  $c$  and  $\omega_I$  are those fitted for  $n = 2$  and  $z_0 = L/8$ . Now the variation of the apex displacement

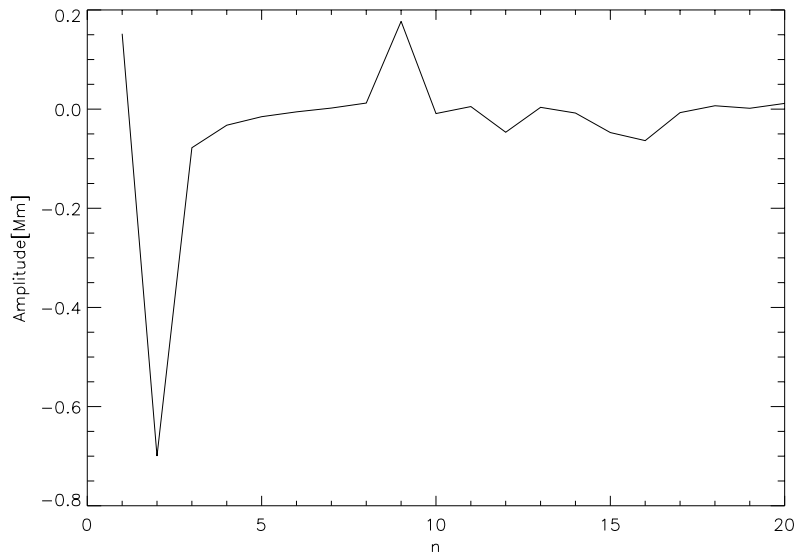


Fig. 9 – Amplitude of the apex displacement of loop 6 as a function of  $n$ .

as a function of  $z_0$  has the profile presented in Figure 10.

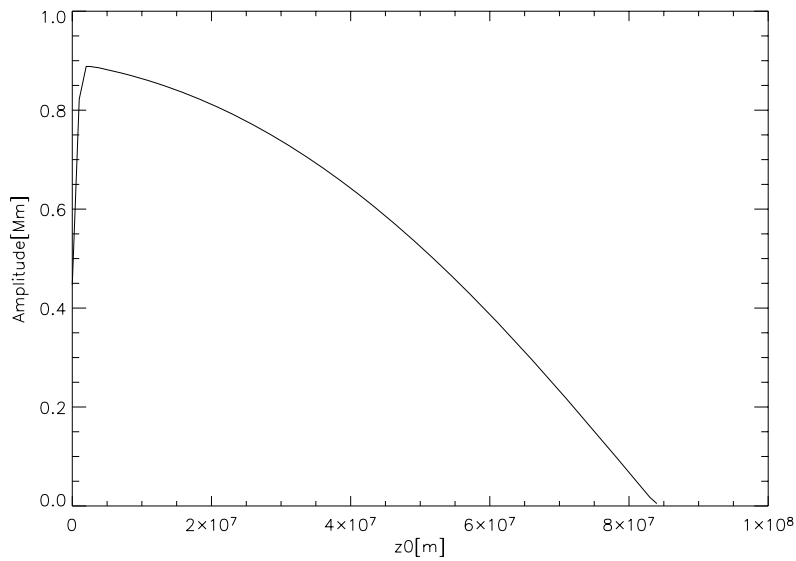


Fig. 10 – Amplitude of the apex displacement of loop 1 as a function of  $z_0$ .

Similarly, if all parameters are held fixed and the values for  $c$  and  $\omega_I$  are those fitted for  $n = 2$  and  $z_0 = L/8$ , then for the particular case of loop 12 the variation of

the apex displacement as a function of  $a$  has the profile presented in Figure 11.

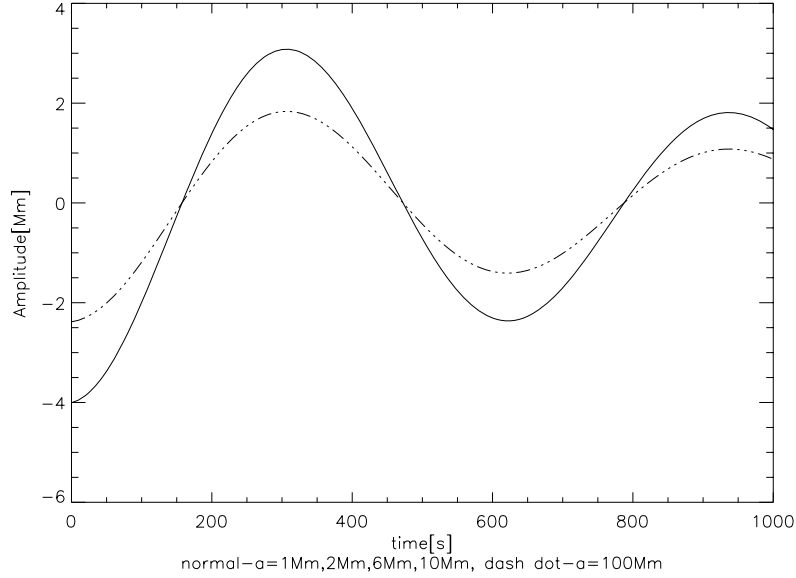


Fig. 11 – Amplitude of the apex displacement of loop 12, as a function of time, with  $a$  as a parameter.

It can be seen that the result shows significant changes only if the interaction width is taken to be very large, i.e. of the order of  $10^8$  m. Obviously such a large value of  $a$  is not realistic, therefore, we consider that for a wide acceptable interval of  $a$ , the width of the interaction does not affect the results.

We also tried to correlate the increase/decrease in the energy needed to displace the loop (within the framework of our model) as a function of the loop length. At the moment this correlation is impossible to establish given the insufficient number or events taken into consideration. For example, if  $z_0 = L/8$  we calculated

$$\Delta = 100 \frac{c_1 - c_0}{c_0}, \quad (13)$$

to be the percentage value of energy increase/decrease needed to displace the loop for  $n = 0$  (through  $c_0$ ) and for  $n = 1$  (through  $c_1$ ). We plotted the quantity  $\Delta$  as a function of loop length  $L$  (see Figure 12). Even though an accurate dependency  $\Delta$  vs.  $L$  cannot be found, at least we can remark that it is generally more efficient to displace a loop with  $n = 1$  than one with  $n = 0$ .

If all parameters are held fixed and the values for  $c$  and  $\omega_I$  are those fitted for  $n = 2$  and  $z_0 = L/8$ , then the variation of the apex displacement as a function of time, with  $z_0$  as a parameter has the profile presented in Figure 15, for loop 4. Even if the

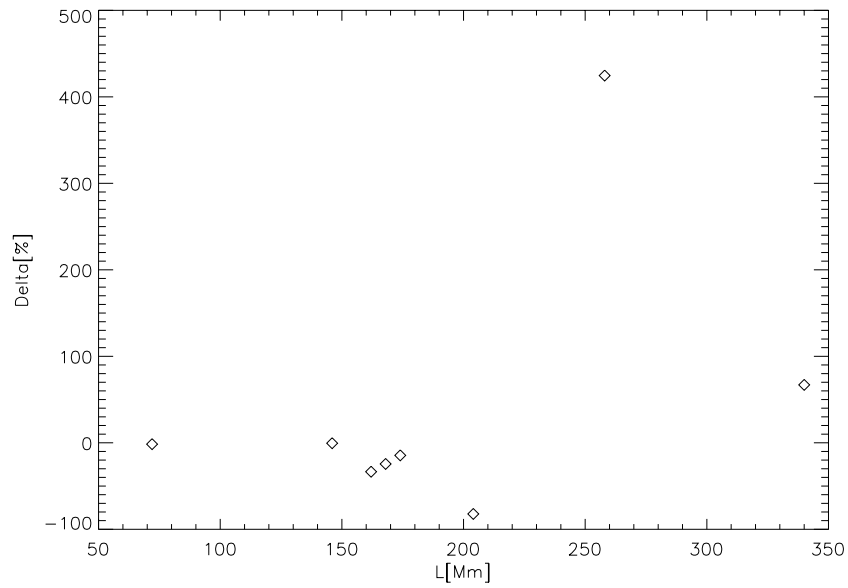


Fig. 12 – Variation with loop length of the supplemental energy needed to displace a loop when  $n$  goes from 0 to 1.

amplitude at a given time and position is the same for a finite interval  $\omega_I$  (Fig. 13), only values fitted in tables 2-9 lead to observed damping times.

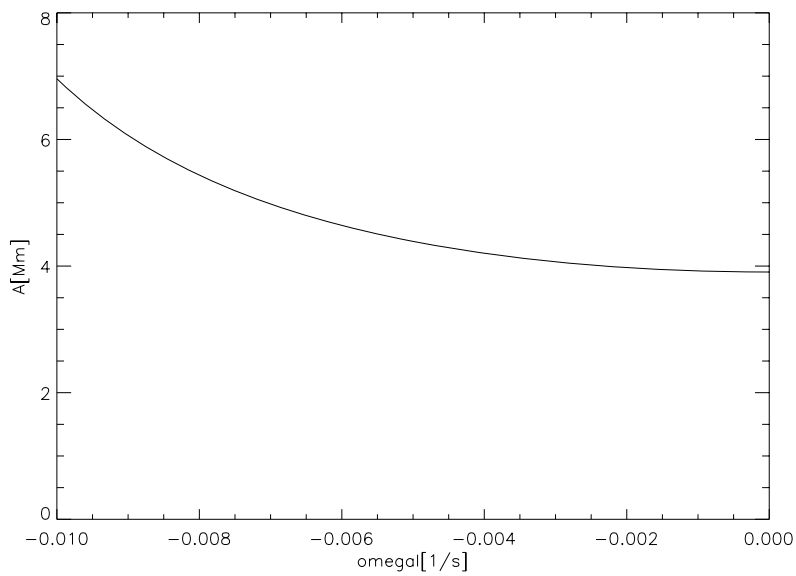


Fig. 13 – Variation of the displacement amplitude as a function of  $\omega_I$ .

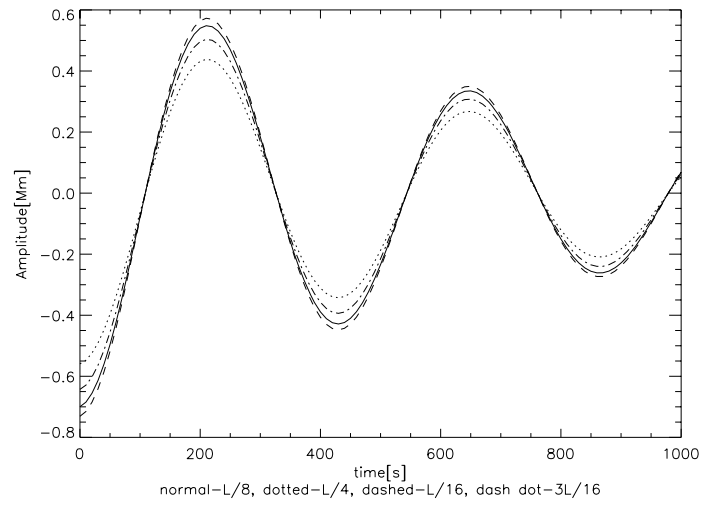


Fig. 14 – Amplitude of the apex displacement for loop 12 deduced by fitting observational points with a damped oscillation.

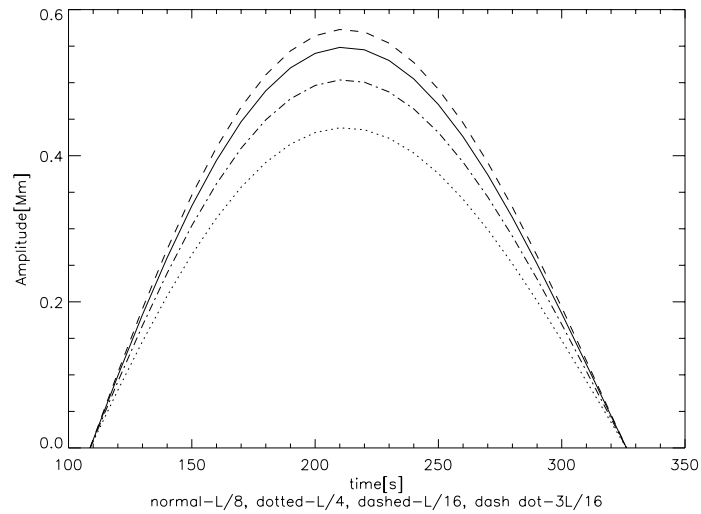


Fig. 15 – Amplitude of the apex displacement for loop 12 according to our model, with  $n = 2$  and  $z_0 = L/8$ .

#### 4. CONCLUSIONS

Our study attempts to present an analytical approach to explain the complicated problem of excitation and damping of transversal coronal loop oscillations. Using observational data we have shown that our proposed model accurately describes the observed behavior of coronal loops following the impact with a shock wave.

The two key points put forward by our model are the analytical shape of the driving force, given by Eq. (9) and the inclusion of a force to account for the opposition of the external magnetized medium to low velocity transversal disturbances. Values obtained for the imaginary part of the frequency,  $\omega_I$ , representing the damping rate of the oscillating loops are within the same order of magnitude for all the analyzed loops, as seen in Tables 2-9. In light of these characteristics of our model we propose that the damping of transversal oscillations is a global characteristic of the solar corona and not something particular to one loop.

The energy transmission coefficient,  $c$ , however, does not present a well defined behavior indicating that a much more complex mechanism for energy absorption and conversion might be at work.

We have also shown that the behavior of the oscillations does not change significantly due to the variable density contrast or a varying width of spatial interaction. For certain values of  $n$  the oscillations may change polarization. However, these values are rather high and it is questionable whether an observational proof of change in polarization may be obtained.

Future work will address the more realistic case when  $\alpha$  is not a global constant, but depends locally on the magnetic properties of the external medium.

#### APPENDIX A. SOLUTION TO THE EVOLUTION EQUATION (8)

The analytical solution to the evolution Eq. (8) is Eq. (12), where the following notations were used

$$A = \frac{2\sqrt{L}}{nv_{A0}\sqrt{\omega_z}} \sqrt{L\omega_z\omega_I^2 - g\omega_R(1 - k_zL) + L\omega_z\omega_R(\omega_z + \omega_R)} = \text{const.}, \quad (1)$$

$$B = \frac{1}{4alnv_{A0}^2} cde^{t\omega_I} LP\sqrt{\pi}(c_{Se}^2 + v_{Ae}^2) \cos t\omega_R = B(t), \quad (2)$$

$$M = J_1(A) \cdot Y_0(e^{n/4}A) - J_0(e^{n/4}A) \cdot Y_1(A), \quad (3)$$

$$I_J(z') = \exp\left\{-\frac{(-z_0 + z')^2}{a^2}\right\} J_0\left(Ae^{nz'/(2L)}\right), \quad (4)$$

$$I_Y(z') = \exp\left\{-\frac{(-z_0 + z')^2}{a^2}\right\} Y_0\left(Ae^{nz'/(2L)}\right), \quad (5)$$

$$T_0(t) = \frac{B(t)}{M}, \quad (6)$$

$$T_1(z) = J_0\left(e^{nz/(2L)}A\right) Y_0\left(e^{n/4}A\right) Y_1(A) \int_1^0 I_J(z') dz', \quad (7)$$

$$T_2(z) = -J_0\left(e^{n/4}A\right) Y_0\left(e^{nz/(2L)}A\right) Y_1(A) \int_1^0 I_J(z') dz', \quad (8)$$

$$T_3(z) = J_1(A) Y_0\left(e^{n/4}A\right) Y_0\left(e^{nz/(2L)}A\right) \int_1^{L/2} I_J(z') dz', \quad (9)$$

$$T_4(z) = -J_0\left(e^{nz/(2L)}A\right) Y_0\left(e^{n/4}A\right) Y_1(A) \int_1^{L/2} I_J(z') dz', \quad (10)$$

$$T_5(z) = -J_1(A) Y_0\left(e^{n/4}A\right) Y_0\left(e^{nz/(2L)}A\right) \int_1^z I_J(z') dz', \quad (11)$$

$$T_6(z) = J_0\left(e^{n/4}A\right) Y_0\left(e^{nz/(2L)}A\right) Y_1(A) \int_1^z I_J(z') dz', \quad (12)$$

$$T_7(z) = -J_0\left(e^{nz/(2L)}A\right) J_1(A) Y_0\left(e^{n/4}A\right) \int_1^0 I_Y(z') dz', \quad (13)$$

$$T_8(z) = J_0\left(e^{n/4}A\right) J_1(A) Y_0\left(e^{nz/(2L)}A\right) \int_1^0 I_Y(z') dz', \quad (14)$$

$$T_9(z) = -J_0\left(e^{n/4}A\right) J_1(A) Y_0\left(e^{nz/(2L)}A\right) \int_1^{L/2} I_Y(z') dz', \quad (15)$$

$$T_{10}(z) = J_0\left(e^{n/4}A\right) J_0\left(e^{nz/(2L)}A\right) Y_1(A) \int_1^{L/2} I_Y(z') dz', \quad (16)$$

$$T_{11}(z) = J_0\left(e^{nz/(2L)}A\right) J_1(A) Y_0\left(e^{n/4}A\right) \int_1^z I_Y(z') dz', \quad (17)$$

$$T_{12}(z) = -J_0\left(e^{n/4}A\right) J_0\left(e^{nz/(2L)}A\right) Y_1(A) \int_1^z I_Y(z') dz'. \quad (18)$$

*Acknowledgements.* GM is supported by the project POSDRU/107/1.5/S/76841.

## REFERENCES

- 1 Aschwanden, M.J., Fletcher, L., Schrijver, C.J., Alexander, D.: 1999, *Astrophys. J.*, **520**, 880.
- 2 Aschwanden, M.J., DePontieu, B., Schrijver, C.J., Title, A.M.: 2002, *Solar Phys.*, **206**, 99.
- 3 Aschwanden, M.J., Nakariakov, V.M., Melnikov, V.F.: 2004, *Astrophys. J.*, **600**, 458.
- 4 Ballai, I.: 2006, *Solar Phys.*, **246**, 177.
- 5 Ballai, I., Douglas, M., Marcu, A.: 2008, *Astron. Astrophys.*, **488**, 1125.
- 6 De Moortel, I., Hood, A.W.: 2003, *Astron. Astrophys.*, **408**, 755.
- 7 De Moortel, I., Brady, C.S.: 2007, *Astrophys. J.*, **664**, 1210.
- 8 DePontieu, B., Martens, P.C.H., Hudson, H.S.: 2001, *Astrophys. J.*, **558**, 859.
- 9 Inglis, A.R., VanDoorsselaere, T., Brady, C.S., Nakariakov, V.M.: 2009, *Astron. Astrophys.*, **503**, 569I.
- 10 McEwan, M.P., Donnelly, G.R., Diaz, A.J., Roberts, B.: 2006, *Astron. Astrophys.*, **460**, 893.
- 11 Nakariakov, V.M., Ofman, L., DeLuca, E.E., Roberts, B., Davila, J.M.: 1999, *Science*, **285**, 862.
- 12 Nakariakov, V.M., Ofman, L.: 2001, *Astron. Astrophys.*, **372**, L53.
- 13 Nakariakov, V.M., Aschwanden, M.J., VanDoorsselaere, T.: 2009, *Astron. Astrophys.*, **502**, 661.
- 14 Ofman, L., Aschwanden, M.J.: 2002, *Astrophys. J.*, **576**, L153.
- 15 Ofman, L.: 2005, *Adv. Space Res.*, **36**, 1572.
- 16 Roberts, B.: 2000, *Solar Phys.*, **193**, 139.
- 17 Ruderman, M.S., Roberts, B.: 2002, *Astrophys. J.*, **577**, 475.
- 18 Safari, H., Nasiri, S., Sobouti, Y.: 2007, *Astron. Astrophys.*, **470**, 1111.
- 19 Schrijver, C.J., Brown, D.S.: 2000, *Astrophys. J.*, **537**, L69.
- 20 Schrijver, C.J., Aschwanden, M.J., Title, A.M.: 2002, *Solar Phys.*, **206**, 69.
- 21 Terradas, J., Oliver, R., Ballester, J.L.: 2005, *Astrophys. J.*, **618**, L149.
- 22 VanDoorsselaere, T., Birtill, D.C.C., Evans, G.R.: 2009, *Astron. Astrophys.*, **508**, 1485.
- 23 Verwichte, E., Aschwanden, M.J., VanDoorsselaere, T., Foullon, C., Nakariakov, V.M.: 2009, *Astrophys. J.*, **698**, 397.
- 24 Wang, T.J., Solanki, S.K., Selwa, M.: 2008, *Astron. Astrophys.*, **489**, 1307.

*Received on 29 February 2012*